NeuroImage 101 (2014) 351–363

Contents lists available at ScienceDirect

NeuroImage

journal homepage: www.elsevier.com/locate/ynimg

Tracing the evolution of multi-scale functional networks in a mouse model of depression using persistent brain network homology

Arshi Khalid [a], Byung Sun Kim [a], Moo K. Chung [b,d], Jong Chul Ye [c,*], Daejong Jeon [a,**]

[a] Brain Behavior and Therapeutics Lab., Department of Bio and Brain Engineering, Korea Advanced Institute of Science and Technology (KAIST), Daejeon, Republic of Korea
[b] Department of Biostatistics and Medical Informatics, University of Wisconsin, Madison, WI 53705, USA
[c] Bio Imaging & Signal Processing Lab., Department of Bio and Brain Engineering, Korea Advanced Institute of Science and Technology (KAIST), Daejeon, Republic of Korea
[d] Waisman Laboratory for Brain Imaging and Behavior, University of Wisconsin, Madison, WI 53705, USA

ARTICLE INFO

Article history:
Accepted 17 July 2014
Available online 24 July 2014

Keywords:
Persistent brain network homology
EEG
Functional connectivity
Depression
Mouse

ABSTRACT

Many brain diseases or disorders, such as depression, are known to be associated with abnormal functional connectivity in neural networks in the brain. Some bivariate measures of electroencephalography (EEG) for coupling analysis have been used widely in attempts to explain abnormalities related with depression. However, brain network evolution based on persistent functional connections in EEG signals could not be easily unveiled. For a geometrical exploration of brain network evolution, here, we used persistent brain network homology analysis with EEG signals from a corticosterone (CORT)-induced mouse model of depression. EEG signals were obtained from eight cortical regions (frontal, somatosensory, parietal, and visual cortices in each hemisphere). The persistent homology revealed a significantly different functional connectivity between the control and CORT model, but no differences in common coupling measures, such as cross correlation and coherence, were apparent. The CORT model showed a more localized connectivity and decreased global connectivity than the control. In particular, the somatosensory and parietal cortices were loosely connected in the CORT model. Additionally, the CORT model displayed altered connections among the cortical regions, especially between the frontal and somatosensory cortices, versus the control. This study demonstrates that persistent homology is useful for brain network analysis, and our results indicate that the CORT-induced depression mouse model shows more localized and decreased global connectivity with altered connections, which may facilitate characterization of the abnormal brain network underlying depression.

Introduction

Depression is one of the most prevalent mood disorders. It is characterized by diverse symptoms including sad mood, loss of interest, and unhappiness, and shows high comorbidity with other brain dysfunction (Banks and Kerns, 1996; Currie and Wang, 2004; DeRubeis et al., 2008; Patten, 2001). Epidemiological studies have shown that depression is common throughout the lifespan of an individual, with 20% of the population worldwide experiencing a depressive episode during their lifetime and 2–5% of the population being affected by severe depression (Kessler et al., 2003, 2005). Depression is unlikely to result from aberrant function of a single gene or brain region (Ressler and Mayberg, 2007). Many studies have reported that numerous regions of the brain are affected by depression, and that the symptoms of depression are associated with the dysregulation of distributed neural networks, encompassing cortical regions, rather than the functional breakdown of a single discrete brain region (Buckner et al., 2009; Davidson et al., 2002a; Drevets et al., 2008; Price and Drevets, 2010; Ressler and Mayberg, 2007; Seminowicz et al., 2004). Thus, to explain in depth the heterogeneous domains of depression symptoms, it is important to use methods that analyze the global functional networks rather than a single region or a local circuit.

Functional connectivity, defined as the temporal correlation between spatially remote neurophysiological events (Friston et al., 1993), is believed to serve as the mechanism for the coordination (or discoordination) of activity between different neural populations or systems across the cortex (Fingelkurts et al., 2005; Friston, 2000). According to recent interpretations of large-scale neural interactions, functional connectivity between the distributed events across the neural networks is important for particular brain actions (Breakspear and Terry, 2002; David et al., 2004; Stam et al., 2003). Electroencephalographic (EEG) signals have been used in the analysis of functional connectivity in patients with depression (Kito et al., 2014; Leuchter et al., 2012; Shafi et al., 2012; Suhhova et al., 2009; Sun et al., 2011). EEG coherence analysis is one of the most widely used approaches to

* Correspondence to: J.C. Ye, Department of Bio and Brain Engineering, Korea Advanced Institute of Science and Technology (KAIST), 291 Daehak-ro, Yuseong-gu, Daejeon 305-701, Republic of Korea. Fax: +82 42 350 4310.
** Correspondence to: D. Jeon, Department of Bio and Brain Engineering, Korea Advanced Institute of Science and Technology (KAIST), 291 Daehak-ro, Yuseong-gu, Daejeon 305-701, Republic of Korea. Fax: +82 42 350 4310.
E-mail addresses: jong.ye@kaist.ac.kr (J.C. Ye), clark@kaist.ac.kr (D. Jeon).

http://dx.doi.org/10.1016/j.neuroimage.2014.07.040
1053-8119/

measuring functional connectivity in coupled neural systems. However, coherence analysis may show increased, decreased, or no change in functional connectivity in the depressed brain (Suhhova et al., 2009). A potential explanation for this varied/unstable result is that coherence determines only the linear characteristics of the EEG time series and can detect only particular sensitivity profiles (Suhhova et al., 2009). Cross-correlation analysis is also used widely for measuring functional connectivity in coupled neural systems. In the correlation approaches to constructing a brain connectivity map, the coupling strengths are decided depending on the optimal threshold level. An issue with these standard methods is that there are no generally accepted criteria for determining the appropriate threshold (Lee et al., 2012), and thus some of the functional connections are not revealed readily (hidden connectivity). To obtain the proper threshold, a multiple-comparison correction over every possible connection could be applicable. However depending on what *p*-value is used for the threshold, the resulting connectome also changes (Bohland et al., 2009; Ferrarini et al., 2009; Rubinov et al., 2009; van Wijk et al., 2010). Thus, it is important for an inclusive approach to ensure the optimal use of the wealth of information present in EEG signals, in seeking to understand the functional dynamics that underlie the mechanism of depression-related symptoms.

Recently, a multi-scale hierarchical network-modeling framework that addressed the problem of determining one optimal threshold was developed; this framework traces the evolution of network changes over different thresholds (Lee et al., 2012). This concept is persistent brain network homology; it handles and analyzes multi-scale networks by identifying the persistent topological features over the changing scales. Using persistent brain network homology with signals from FDG-PET in attention-deficit hyperactivity disorder, it was possible to elaborate functional brain connectivity (Lee et al., 2012; Suhhova et al., 2009).

Although it is difficult to mimic the exact nature of human depression in animals, various animal models showing depression-like behaviors have been developed. These models can help in understanding the pathophysiological mechanisms of human depression (van der Staay et al., 2009). For example, chronic exogenous exposure to corticosterone (CORT) via drinking water in mice stably mimics the increased secretion of glucocorticoids induced by stress exposure in humans, inducing depression-like behavior and neurochemical changes (Ardayfio and Kim, 2006; David et al., 2009; Gourley et al., 2008). Additionally, it has been shown that chronic treatment with antidepressants, such as fluoxetine, can reverse the depression-like phenotype of the CORT model (David et al., 2009; Murray et al., 2008).

In this study, we investigated functional connectivity by applying persistent brain network homology to EEG data from eight cortical regions (frontal, somatosensory, parietal, and visual cortices in each hemisphere) of a CORT-induced mouse model of depression. The hidden brain network in the pathological brain of the CORT model was revealed using the persistent brain network homology technique. We present results that suggest aberrant functional connectivity in the cortical circuitry in the CORT model that may translate into the affective illness of depression.

Material and methods

Animals and generation of the CORT-induced mouse model

Adult male C57BL/6 mice (7–8 weeks old) were used. The animal model of depression was generated by chronic exposure to CORT (Sigma, St. Louis, MO) as described previously (David et al., 2009). Briefly, 35 μg/mL CORT (equivalent to 5 mg/kg/day) was dissolved in drinking water with 0.45% β-cyclodextrin (β-CD, Sigma) for the mice (CORT group). CORT was delivered in light-protected bottles, and was replaced every 3 days for up to 28 days. Control mice received β-CD only (vehicle, VEH group). Mice were housed under a 12/12-h light/dark cycle and had access to food and water ad libitum. Animal care and handling were carried out in accordance with the guidelines approved by the Institutional Animal Care and Use Committee at the Korea Advanced Institute of Science and Technology (KAIST).

Behavioral tasks

Depression-associated behavior tests were conducted: the forced swim task for despair behavior, the elevated plus maze for anxiety, and the open field test for locomotion (Supplementary text and Fig. S1). The results were similar to those in previous reports (David et al., 2009; Gourley et al., 2008). Behavioral experiments were performed after the CORT or vehicle treatment. Behavioral tests were conducted between 4 pm and 8 pm at a light intensity of 80 lx, and were performed as described previously (Jeon et al., 2010; Jung et al., 2013).

Electrode implantation and in vivo electrophysiology for EEG

Animals underwent EEG surgery immediately after the CORT or vehicle treatment. Animals were anesthetized by intraperitoneal injection of ketamine (90 mg/kg) and xylazine hydrochloride (40 mg/kg). Electrode implantation was performed with a stereotaxic apparatus (Kopf Instruments, Tujunga, CA, USA). EEG recordings were obtained with tungsten electrodes (0.005 in. 2 MΩ), positioned in eight cortical regions, based on a mouse brain atlas (Paxinos and Franklin, 2012): frontal cortices (AP +1.5 mm, L ±0.2 mm, and DV −1.0 to −1.1 mm), somatosensory cortices (AP 0.0 mm, L ±1.5 mm, and DV −1.0 to −1.1 mm), parietal cortices (AP −2.0 mm, L ±2.5 mm, and DV −1.0 to −1.1 mm), and visual cortices (AP −3.5 mm, L ±1.5 mm, and DV −1.0 to −1.1 mm) in each hemisphere (Fig. 1). A reference electrode was inserted on the skull above the cerebellum. The electrodes were fixed to the skull with cyanoacrylate adhesive and dental acrylic cement. EEG recordings were combined with video monitoring, and EEG-video recording data were obtained continuously, 24 h/day, for at least 5 days. EEG activity was recorded after the signal was amplified 1200-fold, band pass-filtered at 0.1–70 Hz, and digitized at a sampling rate of 400 Hz using a digital EEG system (Comet XL, Astro-Med, West Warwick, RI, USA). The EEG-video data obtained were analyzed offline using PSG Twin (Astro-Med), Clampfit (Axon Instruments, Foster City, CA, USA), and Matlab (MathWorks, Natick, MA, USA).

EEG analysis and persistent brain network homology

Continuous EEG signals from the animals for three epochs, each consisting of 1 min of data from different days, in which they were in a resting state (i.e., awake and no movement), were analyzed to check the stability of the findings (Supplementary Fig. S3). Then, continuous 1-min-long EEG signals from the last day of recording were used for analyses (Fig. 1b). The five EEG frequency-bands—delta (1.5–4 Hz), theta (4–8 Hz), alpha (8–12 Hz), beta (12–30 Hz), and gamma (30–60 Hz)—were analyzed using a persistent brain network homology approach for functional connectivity.

EEG measurements were obtained in the eight selected ROIs (left frontal cortex, right frontal cortex, left somatosensory cortex, right somatosensory cortex, left parietal cortex, right parietal cortex, left visual cortex, right visual cortex) in ten control mice (β-CD vehicle, VEH group) and nine CORT-drinking mouse models of depression-like behavior (corticosterone, CORT group).

The measurement set was denoted as $M = \{m_1, m_2, \ldots, m_8\}$ consisting of eight nodes (i.e., the eight brain regions) where we had measured m_i at the ith node. We calculated the distance matrix c_M between two EEG measurements m_i and m_j, using the following equation:

$$c_M\left(m_i, m_j\right) = \sqrt{1-\mathrm{corr}\left(m_i, m_j\right)} \quad (1)$$

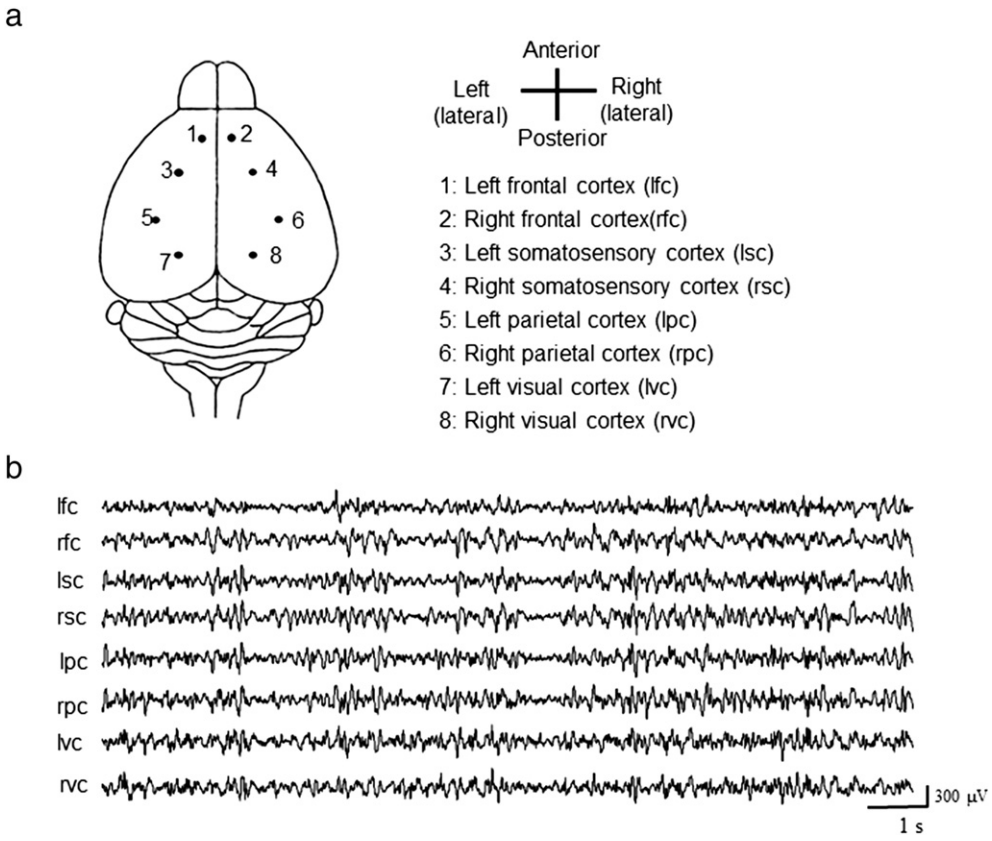

Fig. 1. A schematic drawing of electrode positions and EEG signals. (a) Drawing of a top view of the mouse brain indicating the electrode positions and names of the regions/nodes. (b) Representative original traces of electroencephalogram (EEG) recordings in the eight cortical regions: lfc (left frontal cortex), rfc (right frontal cortex), lsc (left somatosensory cortex), rsc (right somatosensory cortex), lpc (left parietal cortex), rpc (right parietal cortex), lvc (left visual cortex), rvc (right visual cortex), in order.

where $\mathrm{corr}\left(m_i, m_j\right) = \left\langle \frac{m_i}{\|m_i\|}, \frac{m_j}{\|m_j\|} \right\rangle$ refers to the sample correlation between m_i and m_j. Thus, we used the square root of (1-correlation) distance metric to construct binary network.

The brain network can be viewed as a weighted graph (M, c_M) where M is a set of measurements at each brain region (= node) and c_M is the metric defined on that set. We connect the nodes i and j with an edge if the distance $c_M(m_i, m_j) \le \varepsilon$ for some threshold value, ε. Then, the *binary network* B(M,ε) at threshold ε is a graph consisting of the nodes and the edges as depicted in Supplementary Fig. S2b. The binary network B(M,ε) consists of 0-simplices (nodes) and 1-simplices (edges).

Previous studies on brain network modeling used a single fixed threshold, ε, whereas persistent brain network homology is a novel multi-scale hierarchical network modeling framework that traces the evolution of network changes over different thresholds (Lee et al., 2012), starting with $\varepsilon = 0$ and increasing ε at each iteration. The value of ε is taken discretely from the smallest $c_M(m_i, m_j)$ to the largest $c_M(m_i, m_j)$. By increasing ε, more connected edges may become involved. If two nodes are already connected, directly or indirectly, via other intermediate nodes with a smaller ε then at a larger ε they will not be connected. When ε is larger than any distance $c_M(m_i, m_j)$, the iteration terminates because the graph does not change further. Suppose G_k is the graph obtained at the k^{th} iteration with $\varepsilon = \varepsilon_k$. Then, upon changing the threshold, for $\varepsilon_0 \le \varepsilon_1 \le \ldots \le \varepsilon_n$, we obtain a sequence of graphs that correspond to binary networks $B(M,\varepsilon_0)$, $B(M,\varepsilon_1)$, $B(M,\varepsilon_2)$,.... Furthermore, the sequence of graphs follows a hierarchy $G_1 \subset G_2 \subset G_3 \subset \ldots$. Such a sequence of nested graphs is termed a graph filtration in algebraic topology.

More specifically, given a point cloud data M, the *Rips complex* R(M,ε) is a simplicial complex whose k-simplices correspond to unordered $(k + 1)$-tuples of points that are pair-wise within distance ε. Given a point cloud data set consisting of p nodes (i.e., the number of nodes), the Rips complex has at most $(p - 1)$ simplices whereas a binary network has at most 1 simplex (see Supplementary Fig. S2). The Rips complex can also have faces. When ε increases, the subsequent Rips complex becomes larger than all previous Rips complexes. Thus, we have $R(M, \varepsilon_0) \subseteq R(M, \varepsilon_1) \subseteq \ldots \subseteq R(M, \varepsilon_n)$ for $\varepsilon_0 \le \varepsilon_1 \le \ldots \le \varepsilon_n$. The nested sequence of the Rips complex is known as a *Rips filtration*, which is a major theme in persistent homology. A binary network is a subset of the Rips complex (Lee et al., 2012). Thus, we can have a graph filtration for the case of binary networks as $B(M, \varepsilon_0) \subseteq B(M, \varepsilon_1) \subseteq \ldots \subseteq B(M, \varepsilon_n)$.

As shown in Fig. 2(a), as the filtration value, ε, changes, the topological characteristics of the binary network change. The topological change in the filtration can be visualized using the barcode, constructed by plotting the changing topological features over different filtration values. The topological feature is displayed using a bar that starts and ends when the feature appears and disappears. The barcode represents the changes in topological features when the filtration value changes. Among the many topological features, here, the zeroth Betti number, which counts the number of connected components in a network, is our interest. Because the pth Betti number is estimated by the p- and $(p + 1)$-simplices, the binary network B(M,ε) contains enough information to compute β_0. In Fig. 2(b), we plotted the zeroth Betti number β_0 (vertical axis) of the Rips complex over the filtration values $\varepsilon_0, \varepsilon_1, \ldots, \varepsilon_n$ (horizontal axis).

Other brain network studies, such as characteristic path length, clustering coefficients, assortativity, and modularity, focus on reflecting different topological characteristics of the brain network and measuring similarities between them. These measures quantify the network properties after all nodes are connected. However, the change in β_0 shows topological changes in a network before all nodes are connected.

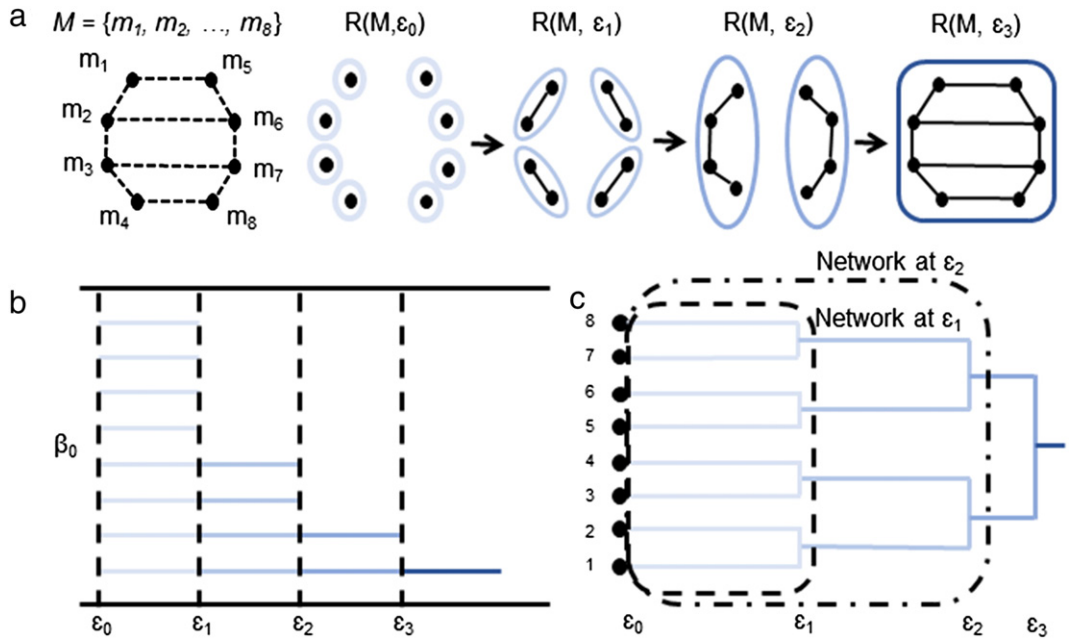

Fig. 2. Schematic drawing of network evolution over increasing filtration values, ε_0, ε_1, ε_2, and ε_3. (a) Node set M and the Rips filtration at filtration values ε_0, ε_1, ε_2, and ε_3; (b) barcode showing the changing topological features. The y-axis is the zeroth Betti number (counts the number of connected components) and filtration values are shown on the x-axis. (c) Single-linkage dendrogram (SLD) indicating geometrical information on subnetwork formation before merging into one large connected component.

While the barcode in Fig. 2(b) represents global topological changes in a network, rearranging the bars in the barcode and connecting the bars according to the node index and the Rips filtration, we obtain a single-linkage dendrogram (SLD).

Consider the Rips filtration. Let C_m^k and C_n^k be the two disconnected components of the Rips complex R(M, ε_k). Suppose there exist two nodes m_i in C_m^k and m_j in C_n^k such that the distance d between them is less than the next filtration value ε_{k+1}. Then, these two disconnected components will be connected at ε_{k+1} if

$$d\left(C_m^k, C_n^k\right) = \min_{x_i \in C_m^k, x_j \in C_n^k} d\left(x_i, x_j\right) < \varepsilon_{k+1}.$$

The sequence of merged components during the Rips filtration is identical to the sequence of the merging in dendrogram construction (Lee et al., 2012). The linking of two nodes corresponds to merging two leaves in the dendrogram.

Regardless of which node we start with, a consistent dendrogram is always generated. In Fig. 2(c), the SLD shows the local network characteristics of the subnetworks that are clustered together at earlier filtration values before merging into one large component. Using SLD, we can recompute the distance between the nodes in the network using the single-linkage distance, a model predictive distance using SLD. Mathematically the single-linkage distance is given by:

$$d_M\left(m_i, m_j\right) = \min\left\{\max_{l=0,\cdots,k-1} c_M\left(w_l, w_{l+1}\right) / m_i = w_0, \cdots, w_k = m_j\right\} \quad (2)$$

where $m_i = w_0, \ldots, w_k = m_j$ is a path between m_i and m_j.

Statistics

For intergroup comparisons of behaviors, Student's *t*-test was used, and all data for behaviors are presented as means ± standard error of mean (SEM). A p-value <0.05 was considered to indicate statistical significance. The Mann–Whitney U-test and the Wilcoxon rank-sum test were used for intergroup comparisons of EEG data. The SPSS software (ver. 21.0; SPSS Inc., Chicago, IL) and Matlab were used for statistical analyses.

For the calculation of p-values of slopes and final filtration values in the barcode, we resampled the correlation matrix of each subject using bootstrapping (1000 replications), and obtained the slopes and final filtration values of the barcode based on resampled data sets. Then, the Wilcoxon rank-sum test was performed for the statistical comparison of slopes and final filtration values of the barcodes between the groups. The Mann–Whitney–Wilcoxon test was used to compare pair-wise single-linkage matrices with a Bonferroni correction.

Results

We computed correlation-based distance matrices c_M (1) for the CORT and VEH groups (Fig. 3). Each ijth entry in the distance matrix is a correlation-based functional distance between two nodes m_i and m_j, calculated with Eq. (1). Visually, neither group displayed a clear separation of clusters arising from regional couplings (Fig. 3).

Next, we applied the persistent homology approach to explore functional connectivity at the network level for each frequency band of the EEG data recorded from the CORT and VEH groups. We obtained the persistent topological features in the brain network, changing over increasing filtration values using barcodes. Filtration was performed between 0 and 1 because all of the brain regions or nodes merged together before filtration reached 1, eliminating the need to consider distance values larger than 1. Based on the barcodes, we also constructed connectivity maps to incorporate the geometrical information about the positions of the connected nodes (the eight brain regions). Furthermore, we computed single-linkage distance matrices and the dendrogram for the predicted distances between the eight nodes and for the single-linkage hierarchical clustering, respectively.

Fig. 4(a–c) shows the connectivity map and barcode at the delta-frequency band for the VEH and CORT groups. In Fig. 4(c), the overlaid barcodes are presented for the intergroup comparison between the VEH and CORT groups. The CORT group showed an increased number of connected components (zeroth Betti number, β_0) at filtration values from 0.4 to 0.8 in the barcode versus the VEH group. The maximum single-linkage distances (i.e., the final filtration value) of the VEH and CORT groups were 0.7281 and 0.7979, respectively. The final filtration value for the two groups were CORT > VEH at 95% level of confidence (tested with the Wilcoxon rank-sum test for resampled datasets,

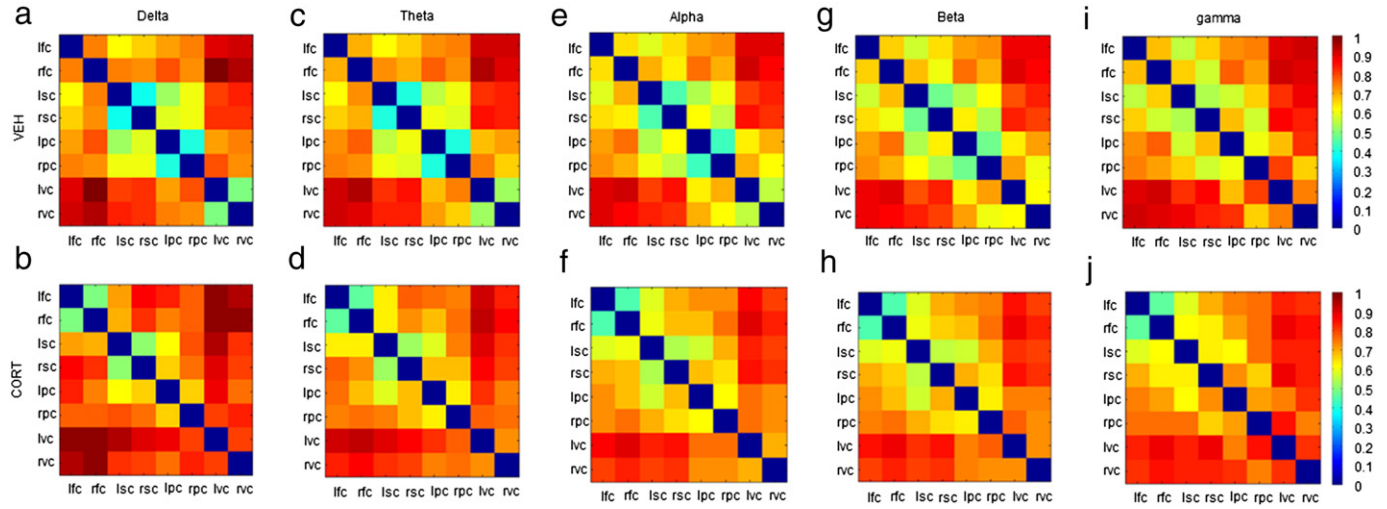

Fig. 3. Distance matrices indicating statistical dependencies. Correlation-based distance matrices at delta-, theta-, alpha-, beta-, and gamma-frequency EEG bands in the VEH (a, c, e, g, and i) and CORT groups (b, d, f, h, and j). The distance matrices provide visually inefficient information for ascertaining group differences.

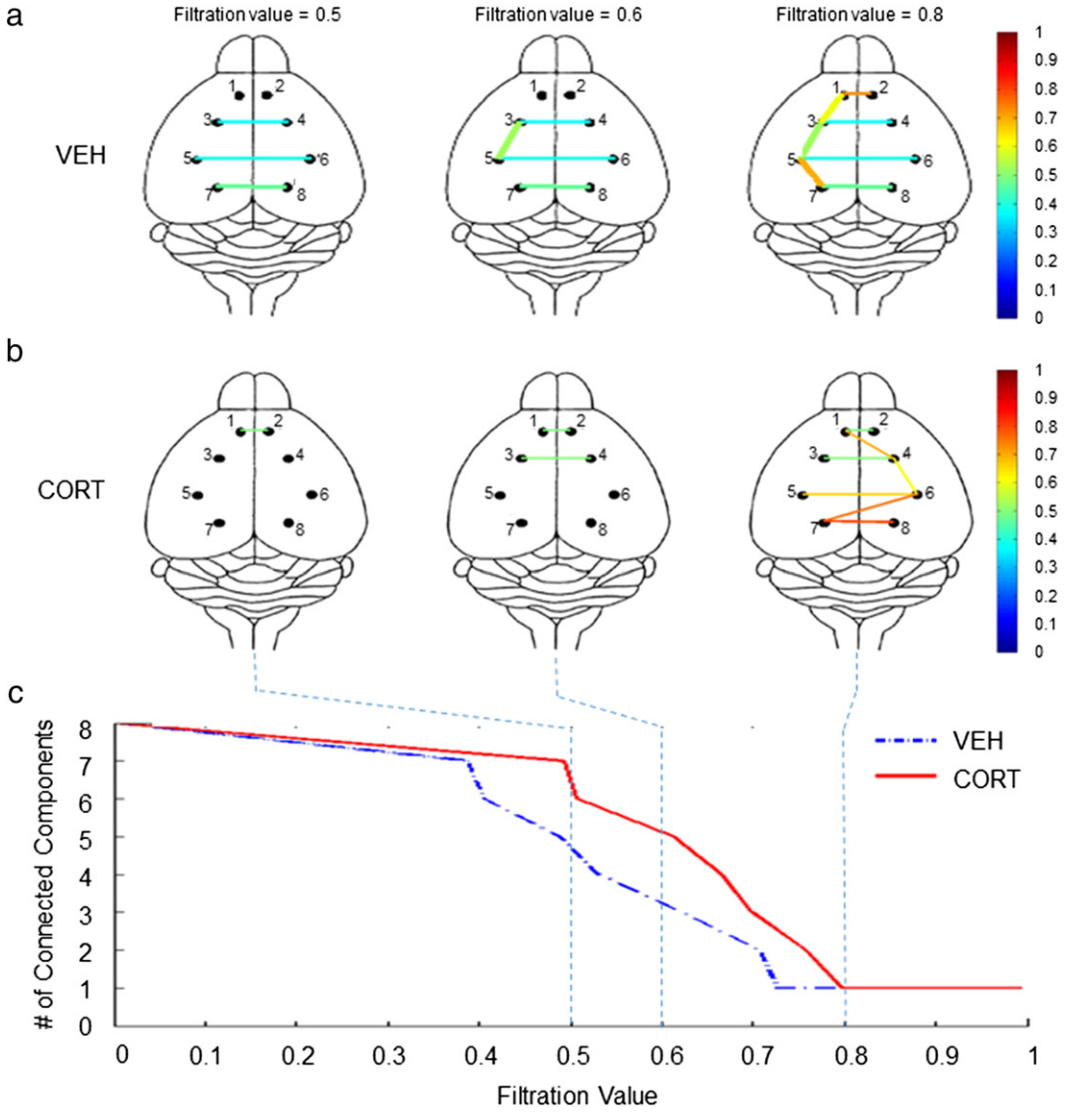

Fig. 4. Trace of network evolution over changing filtration values in the delta-frequency band. Connectivity maps of the VEH (a) and CORT (b) groups at filtration values $\varepsilon = 0.5$, 0.6, and 0.8, where color strength in the color bar represents the functional distance between the nodes. Altered and decreased functional connectivity in the CORT group is seen in the brain network connectivity map. The overlaid barcodes of the VEH and CORT groups show brain network evolution over the different filtration values in (c) where the final filtration value of the CORT group ($=0.7979$) > the VEH group ($=0.7281$) at the 95% level of confidence (Wilcoxon rank-sum test of resampled data sets). Thus, the CORT group with a longer, heavy tail exhibited decreased global connectivity at the 95% level of confidence.

when resampling was performed using a bootstrap approach). These results indicate decreased global connectivity in the CORT group. Taken together, the higher β_0 with changing filtration values and the longer heavy tail in the shape of the barcode of the CORT group indicate more localized and decreased global connectivity. Moreover, the decreasing slopes of the barcodes were slope CORT ($=18.1871$) > slope VEH ($=15.6128$), with a significance level of 0.05 (Wilcoxon rank-sum test for resampled data sets). Here, interpretation of local connectivity should not be confused with the criteria for reading the barcode graph for global connectivity, which is how a large subnetwork is reached at an earlier threshold. Local connectivity is an indicator of how many local connected clusters there are at a particular filtration value. For example, the VEH group had four local clusters of connected components at a filtration value of 0.6. However, the CORT group had six local clusters of connected components at the same value (Fig. 4), indicating a more localized connectivity. The connectivity maps at three different values ($\varepsilon = 0.5, 0.6, 0.8$) from the barcodes are shown in Fig. 4(a–b). The color of the color bar is simply a filtration value, serving as an edge weight between two connected nodes. A lower filtration value, or a cooler color indicates increased connectivity and less functional distance, whereas a high filtration (anti-correlation) value indicates decreased connectivity and a higher functional distance. The altered connectivity pathways of the CORT group can be visualized readily using geometrical maps. The decreased connectivity at each filtration value indicates hypoactivation of the final network in the CORT group.

Fig. 5(a–b) shows a single-linkage matrix for the delta-frequency band of the VEH and CORT groups, illustrating the functional distance between the brain regions. This single-linkage matrix could produce efficient separation of the brain subnetworks within each group, compared with the correlation-based distance matrices shown in Fig. 3. Each ijth entry in the single-linkage matrix is a model-based predicted functional distance between the two nodes, m_i and m_j. The Mann–Whitney test for exact probabilities was used to assess the difference in subnetworks between the groups. The model-predicted distances from single-linkage matrices were tested with the Mann Whitney test at the 0.05 level of significance assuming heterogeneity of variances of the two groups. For pair-wise comparisons of single-linkage distances, the Wilcoxon rank-sum test was used with Bonferroni's correction. It was found that the CORT group showed increased distances among the somatosensory, parietal, and frontal regions versus the VEH group, indicating looser coupling or decreased connectivity in those regions in the CORT group (corrected $p < 0.01$). Loosely connected visual cortices in the CORT group were also indicated in the single-linkage distance matrices (corrected $p < 0.01$). Additionally, it was observed that the left frontal and left/right somatosensory and parietal cortices were further apart functionally in the CORT group than in the VEH group, indicating reduced connectivity in the CORT group (corrected $p < 0.01$). We visualized the geometrical information about the altered brain network by computing a dendrogram (Fig. 5c–d). The dendrogram provides a visual representation of how and where the brain network changes. The colors of the lines in the dendrogram represent the distance to the 'giant'

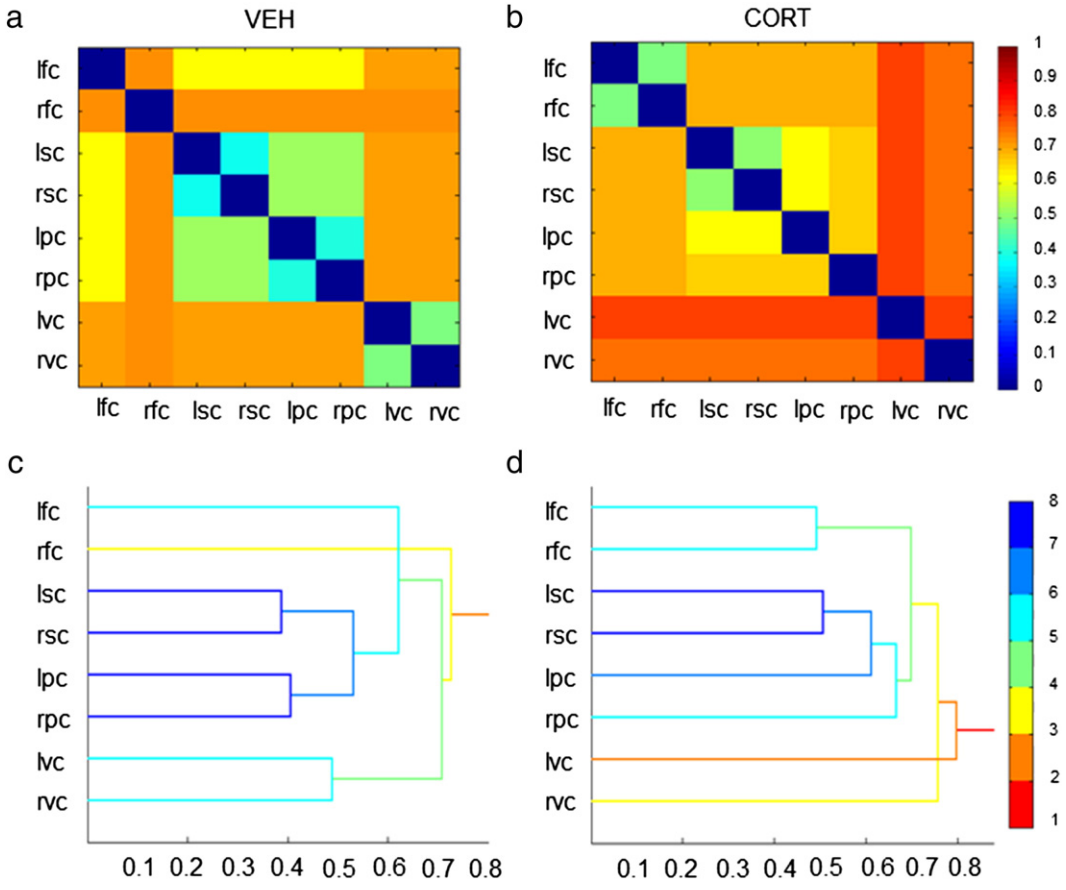

Fig. 5. Increased functional distance and decreased functional connectivity visualized using single-linkage matrices and a dendrogram in the CORT group. (a, b) Single-linkage matrices (SLMs) d_M for the delta-frequency band of the VEH and CORT groups, with a better illustration of group separation than the original distance matrices obtained from the Pearson correlation-based distance c_M in Fig. 3. Intergroup comparison showing loose coupling between somatosensory and parietal cortices (among the cortical circuitries of the CORT group other than the right frontal cortex and other regions) at the 0.01 level of significance (two-tailed Mann–Whitney test for exact probabilities). The single-linkage dendrograms for the VEH and CORT groups are presented in (c, d). The vertical and horizontal axes represent the node index and filtration value, respectively. The line colors indicate the distance to the giant component. The distance to the giant component is 1. Differing subnetwork formation over the changing filtration values can be seen in both groups. Hyperconnectivity in the frontal cortices and hypoconnectivity in the visual cortex in the CORT group can be seen from the dendrograms of both groups. Also, the somatosensory cortices in the CORT group make connections with other cortical circuitry at later filtration values, resulting in decreased connectivity.

component (one final component in which all nodes are connected to each other) for each connected component. The dendrogram at the delta frequency revealed decreased coupling (at earlier filtration values, $\varepsilon = 0.6$–0.8) among the brain regions of the CORT group versus the VEH group. In the CORT group, a subnetwork consisting of somatosensory and parietal regions was formed at a higher filtration value (Fig. 5d), while the same subnetwork was established at an earlier filtration value in the VEH group (Fig. 5c). This result indicates that in the CORT group, more local clusters are present at earlier filtration values, while not forming a big network.

With the persistent homology analysis at the theta- (Fig. 6), alpha- (Fig. 7), beta- (Fig. 8), and gamma-frequency bands (Fig. 9), we also found similar functional connectivity trends to the results for the delta-frequency band analysis in the CORT group (i.e., significantly decreased global connectivity and more localized connectivity, as shown in the barcodes; Figs. 6–9). Furthermore, decreased functional connectivity of

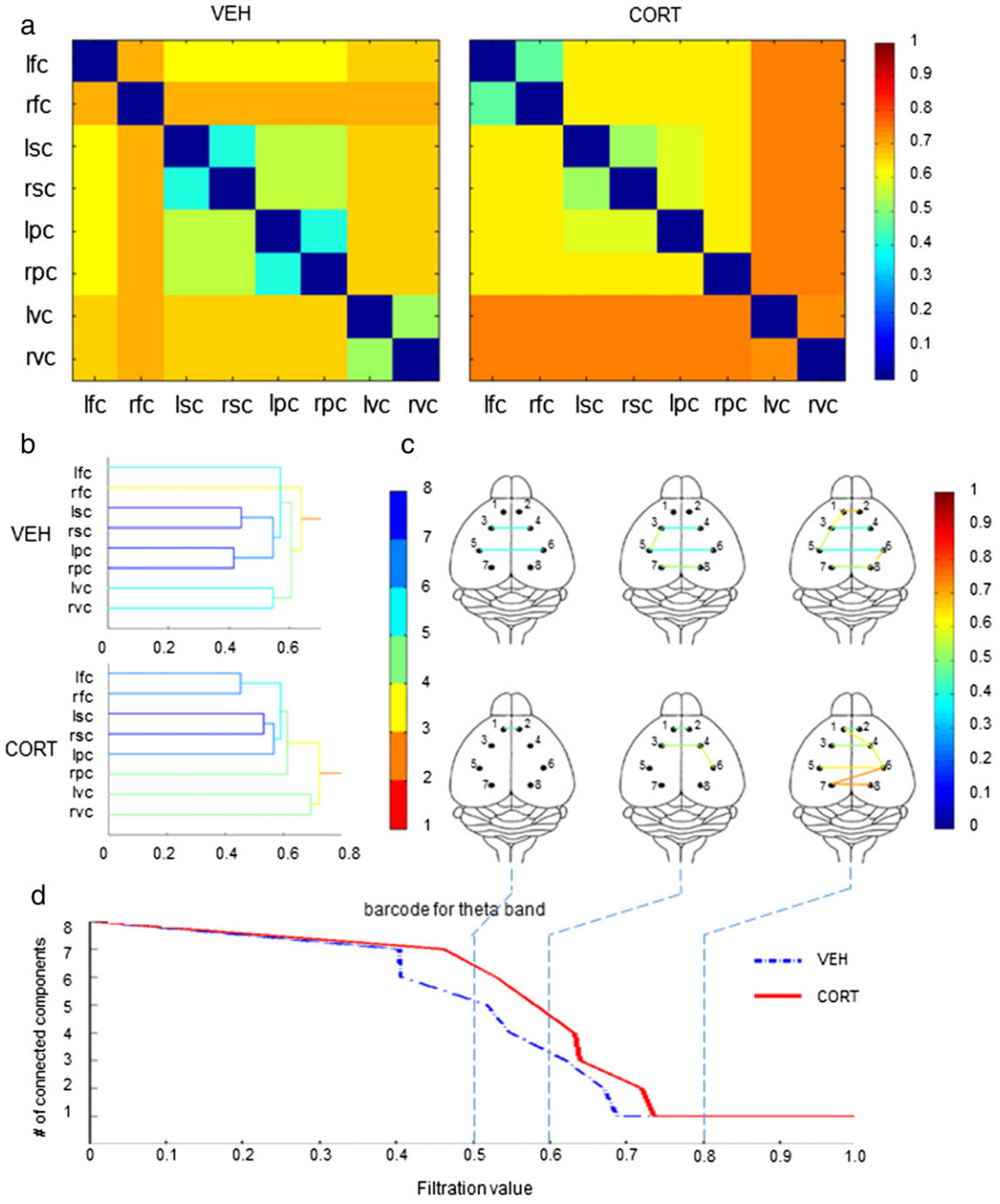

Fig. 6. Trace of network evolution over changing filtration values in the theta-frequency band. (a) Single-linkage matrices (SLMs) d_M for theta frequency in the VEH and CORT groups. The loose coupling among the various brain regions in the CORT group is seen and was verified using the Mann–Whitney test for exact probabilities. Single-linkage dendrograms for the VEH and CORT groups are presented in (b). The vertical and horizontal axes represent the node index and filtration values, respectively. The line colors indicate distance to the giant component. The distance to the giant component is 1. (c) Connectivity maps of the VEH group and CORT groups at filtration values of $\varepsilon = 0.5$, 0.6, and 0.8, where color strength in the color bar represents the functional distance between nodes. Altered and decreased functional connectivity in the CORT group is seen in the brain network connectivity map. The overlaid barcodes of the VEH and CORT groups trace brain network evolution over the different filtration values in (d) where the final filtration value of the CORT group ($=0.7357$) > the VEH group ($=0.6770$) at the 95% level of confidence (Wilcoxon rank-sum test of resampled data sets). Thus, the CORT group shows decreased global connectivity at the 95% level of confidence.

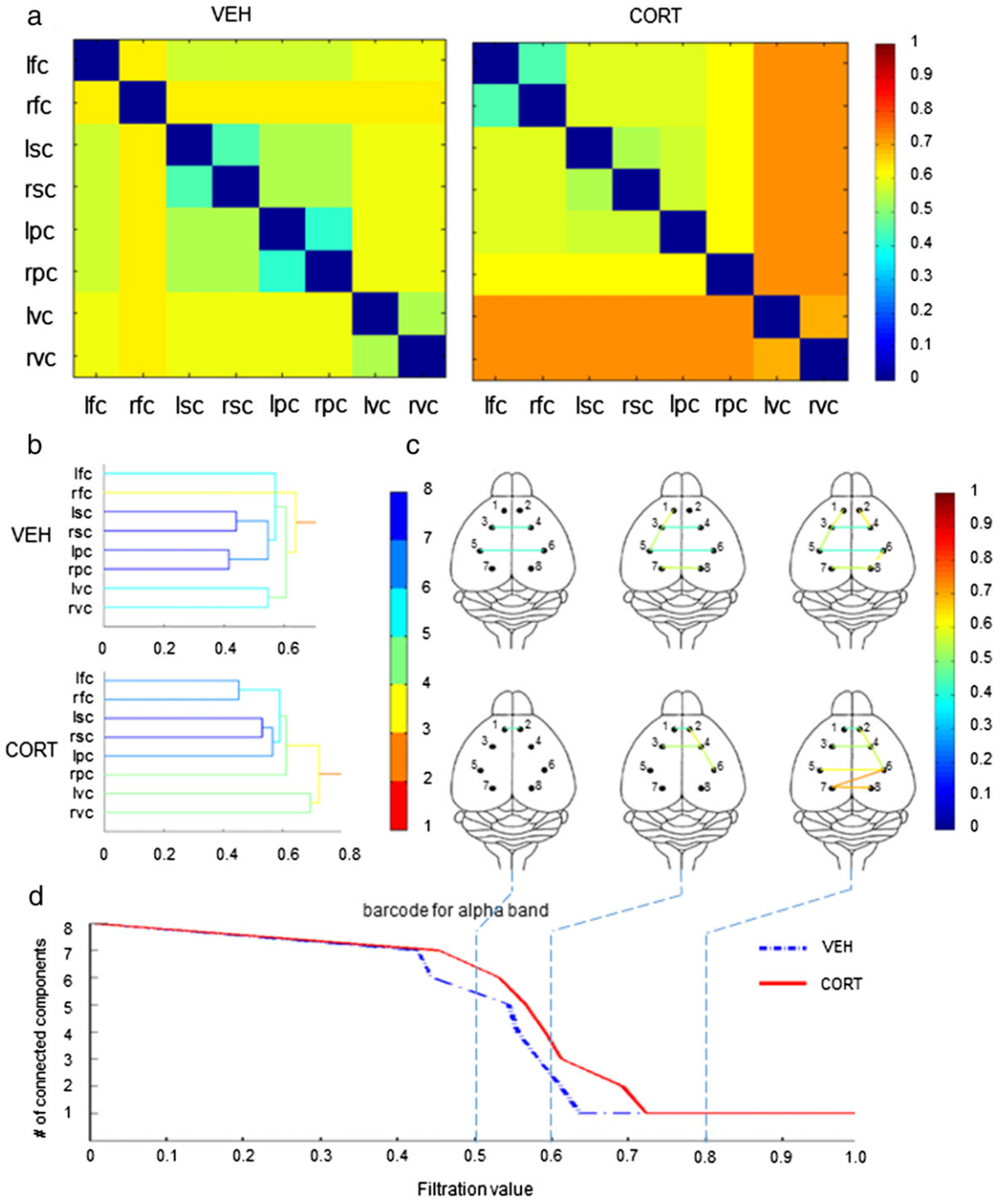

Fig. 7. Trace of network evolution over changing filtration values in the alpha-frequency band. (a) Single-linkage matrices (SLMs) d_M of the VEH and CORT groups are presented in (a, b). An intergroup comparison was performed statistically at the 0.05 level of significance (Mann–Whitney two-tailed test for exact probabilities). Single-linkage dendrograms for the VEH and CORT groups are presented in (b). The vertical and horizontal axes represent the node index and filtration values, respectively. The line colors show the distance to the giant component. The distance to the giant component is 1. Altered connections in the CORT group versus the VEH group are seen clearly in the dendrogram representation. (c) Connectivity maps of the VEH and CORT groups at filtration values of $\varepsilon = 0.5$, 0.6, and 0.8, where color strength in the color bar indicates the functional distance between the nodes. Altered and decreased functional connectivity in the CORT group is seen in the brain connectivity map. Also, in the alpha-frequency band, altered trends in somatosensory circuits with the parietal and frontal cortices are evident from the connectivity map at a filtration value of 0.5 in both groups. The overlaid barcodes of the VEH and CORT group show brain network evolution over the different filtration values in (d) where the final filtration value of the CORT group (=0.7224) > the VEH group (=0.6362) at the 95% level of confidence (Wilcoxon rank-sum test of resampled data sets). Thus, the CORT group exhibited decreased global connectivity with a 95% level of confidence.

the CORT group was revealed and visualized at the theta-, alpha-, beta-, and gamma-frequency bands by single linkage distance matrices (Figs. 6a, 7a, 8a, 9a) and dendrograms (Figs. 6b, 7b, 8b, 9b).

In Fig. 6(a) model-predicted distance matrices (i.e., single-linkage matrices) for the theta-frequency EEG bands are shown. Decreased functional connectivity in the CORT group was seen among the various brain regions. Statistically significant pair-wise differences between the groups were shown using the Wilcoxon rank-sum test. In Fig. 6(b) dendrograms for the theta-frequency EEG band are shown. In Fig. 6(c), brain connectivity maps for the theta frequency are presented. From the geometrical information on connected nodes, the CORT group showed similar results to those of the delta-frequency band (i.e., more local clusters until higher filtration values). It can be seen that the connectivity map of the CORT group shows compromised coupling among brain regions at earlier

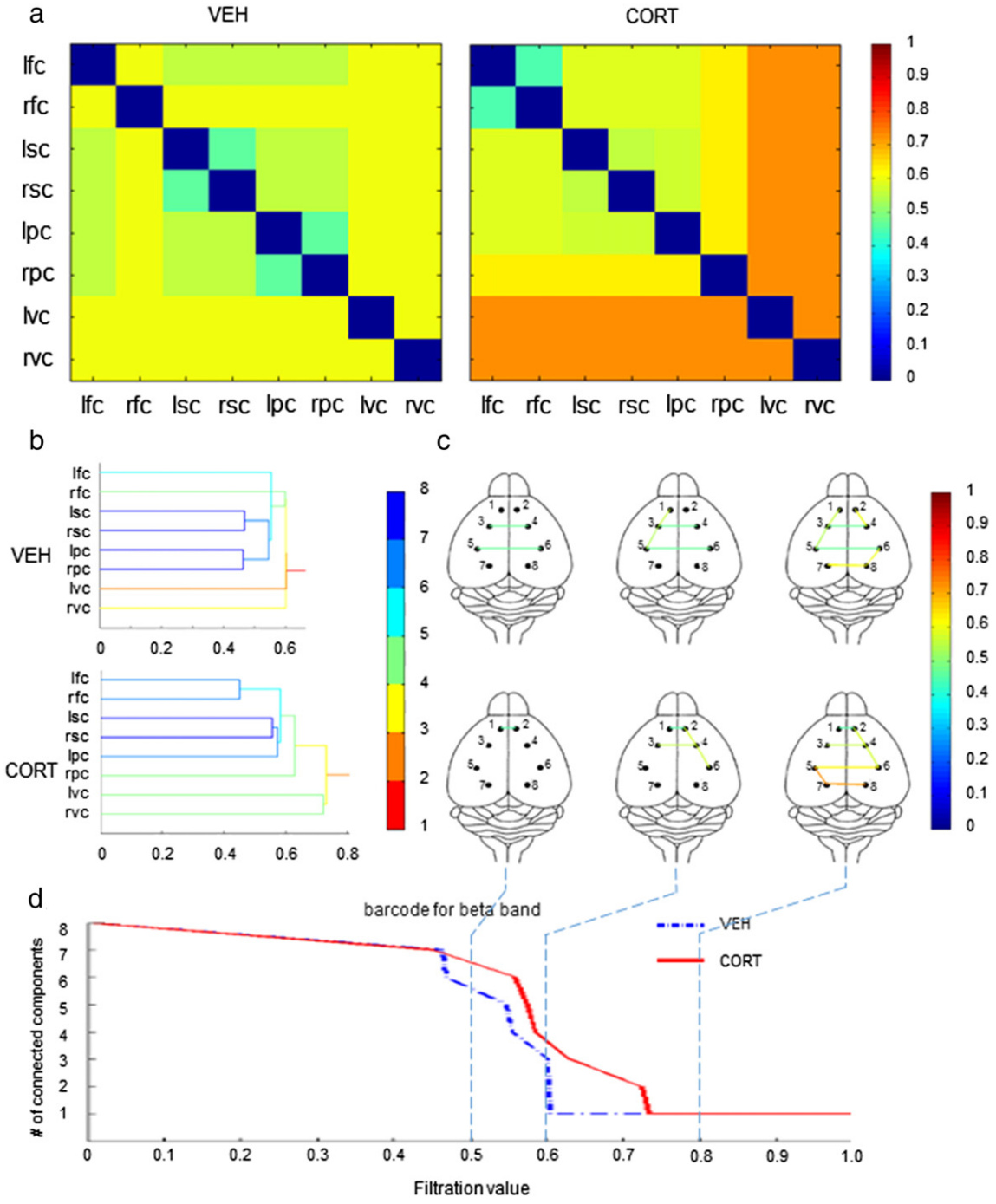

Fig. 8. Network findings in the beta-frequency band. (a) Single-linkage matrices for both groups are presented, VEH (left) and CORT (right). (b) The single-linkage dendrogram showed altered connections among the nodes of the CORT group (below) when compared with the VEH group (upper). (c) Brain connectivity maps show increased local connectivity and decreased global connectivity in the CORT group. (d) Overlaying the barcodes in both groups shows significantly decreased global connectivity in the CORT group with a long tail after the final filtration value: CORT (0.7329) > VEH (0.6037) at the 95% level of confidence (Wilcoxon rank-sum test).

threshold values (0.5, 0.6) and decreased connectivity strength at 0.8 compared with the VEH group. Cortical regions in the CORT group were making fewer connections in the evolution of the final network, as they became one large component at higher filtration values than in the VEH group. In the theta-frequency band, overlaying the barcodes along with the final filtration values (CORT group, 0.735; VEH group, 0.677) revealed significantly decreased global connectivity (0.05 level of significance, using the Wilcoxon rank-sum test on resampled data sets) in the CORT group (Fig. 6d). Furthermore, slope (CORT = 21.57) > slope (VEH = 18.16), which suggests that the CORT group had a more rapidly decreasing slope than the VEH group. Thus, the slope of the barcodes may not be useful when making inferences on the shape of barcodes.

The barcodes for the alpha-, beta-, and gamma-frequency bands and their slopes (CORT, 23.04 and VEH group, 25.49, CORT, 21.228 and VEH group, 33.29, and CORT, 21.47 and VEH group, 34.84, respectively) all showed that the VEH group had a steeper slope than the CORT group, yielding a faster decrease of the zeroth Betti number, or increased global connectivity in the VEH group. Furthermore, the final filtration values (alpha: CORT, 0.72 and VEH group, 0.63, beta: CORT, 0.6037 and VEH group, 0.7329, and gamma: CORT, 0.6847 and VEH group, 0.7489) revealed that the CORT group had a longer, heavy tail, indicating

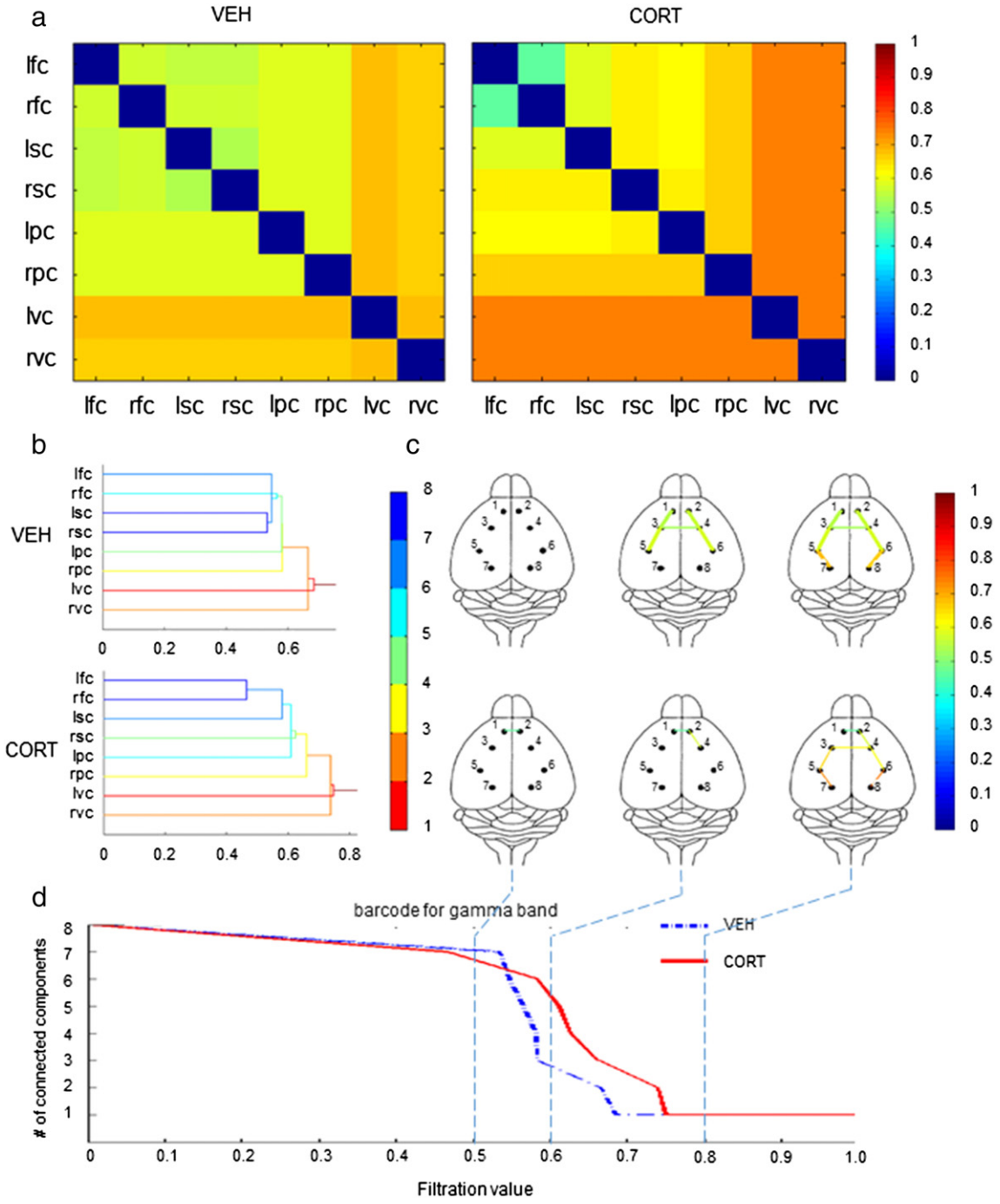

Fig. 9. Network findings at the gamma band. A similar connectivity profile to the other four frequency bands was seen: decreased global connectivity among the cortical circuitry in the CORT group. (a) Single-linkage matrices are presented for both groups: VEH (left) and CORT (right). (b) Single-linkage dendrogram shows altered connections among the nodes in the CORT group (below) versus the VEH group (upper). (c) Brain connectivity maps show increased local connectivity and decreased global connectivity for the CORT group. Also, hyperconnectivity in the frontal cortices is evident at earlier filtration values (=0.5). (d) Overlaying the barcode in both groups showed significantly decreased global connectivity in the CORT group with a long tail since the final filtration value for CORT (0.7489) > VEH (0.6847) at the 95% level of confidence (Wilcoxon rank-sum test).

decreased global connectivity and more localized connectivity in the alpha, beta, and gamma frequency ranges (Figs. 7d, 8d, 9d). In Figs. 7(a), 8(a), and 9(a), the model-predicted distance matrices (single-linkage matrices) for alpha-, beta-, and gamma-frequency EEG bands are shown, respectively.

Decreased functional connectivity in the CORT group was shown among almost all the distinct brain regions. The statistical significance of differences between groups was assessed using the Mann–Whitney test for exact probabilities with a Bonferroni correction. In Figs. 7(b), 8(b), and 9(b), dendrograms for the alpha-, beta-, and gamma-frequency EEG bands are shown, respectively. Alpha-, beta-, and gamma-frequency-specific brain connectivity maps and other findings are also shown in Figs. 7(c), 8(c), and 9(c), respectively. Similar connectivity profiles (decreased global and increased localized connectivity in the CORT group) but with different pathways among the cortical regions were seen in all five EEG frequency bands. Interestingly, the bilateral frontal cortices in the CORT group showed increased connectivity in the CORT group versus the VEH group at all five bands, which might

indicate the spread of depression severity because depression is characterized by increased functional connectivity within the frontal brain (Olbrich et al., 2014).

Comparison with other graph theoretic measures

To validate the approach of persistent brain network homology with other available graph theoretic approaches, we constructed 10 and 9 networks for the VEH and CORT groups, respectively. For all $(10 + 9)$ networks, we obtained seven distance matrices between the networks, including the Gromov–Hausdorff distance (Supplementary material), between all pair wise single-linkage matrices along with pair wise differences between six other graph theoretic measures: the slope of barcode β_0, the characteristic path length, the average assortativity, the average clustering coefficient, the modularity, and average node betweenness centrality (Supplementary Fig. S4). All distance matrices were normalized to have a maximum value $= 1$. After constructing the distance matrices, we divided the networks into two clusters and evaluated the clustering accuracy by comparing the assigned labels with the true labels. The clustering accuracies of the GH distance and the characteristic path length were both 100%, superior to the other widely used graph theoretic measures, indicating effective performance of the GH metric (Supplementary Fig. S4).

Discussion

To assess brain functional connectivity, persistent brain network homology, a new multi-scale network-modeling framework (Lee et al., 2012), was used effectively with EEG signals from the CORT-induced depression mouse model. Persistent brain network homology uses networks generated at every possible threshold, and thus eliminates the need for an optimal threshold, which is a key factor in constructing binary networks. Furthermore, the persistent homology approach can allow geometric information in the barcode to be incorporated into a single-linkage dendrogram that represents the brain network changes visually. Thus, 'hidden' or abnormal neural networks in the pathological brain can be revealed by the persistent brain network homology approach.

In this study, application of persistent homology in eight cortical regions revealed more localized and decreased global connectivity in the CORT group versus the VEH group. Additionally, connectivity maps with single-linkage distances showed reduced and highly discriminated functional connectivity in the subregions in the CORT group. Our study demonstrated less integrated processing of effective information in cortical brain regions of the CORT group, and our results may facilitate investigation of the mechanisms underlying aberrant neural networks in the depressed brain.

Functional connectivity in the brain can be measured by statistical dependencies among the physiological signals from the coupled neural systems. In the healthy brain, individual variability in cognitive functions, learning a new task, and even the predisposition to learn have been correlated with specific patterns of connectivity within/across networks. In the diseased brain, specific abnormalities in neural networks even in structurally normal regions, may correlate with functional deficits, and functional connectivity has been used to assess impairment in neural communications (Fox et al., 2005; He et al., 2007a,b; Shafi et al., 2012). Depression may be associated with disturbed properties across large-scale cortical networks and/or subcortical systems with a number of functionally connected cortical regions (Davidson, 2004; Davidson et al., 2002b). Measurement of electrical activity, such as by EEG, has been used for research into brain functional connectivity, and many studies have suggested that alterations in EEG functional connectivity of patients with brain disorders, including depression, may be associated with cognitive dysfunction and psychiatric behaviors (Dawson, 2004; Haig et al., 2000). However, tracing global networks through the evolution of local subnetworks, where selection of the optimal threshold can be a problem, is difficult.

The persistent homology analysis, with the help of barcodes at all five EEG frequency bands, showed a more localized and decreased global connectivity in the CORT mouse model. Additionally, the geometrical information-based dendrogram showed altered and compromised functional pathways in the somatosensory, frontal, and parietal cortices during formation of a large network. In fact, there is a report that patients with depression have limited affective processing and fewer redundant, or simply a reduced number of, connections among those cortical regions (Leistritz et al., 2013). At each frequency band, a single-linkage distance matrix showed decreased connectivity among the left frontal and parietal cortices of the CORT group. Because the parietal lobes are themselves closely interconnected with the prefrontal areas, and, together, these two regions represent the highest level of integration in the motor control hierarchy, decreased connectivity in these regions may lead to impairment in cognitive function, including decision-making. Moreover, bilaterally looser connection at the visual cortex and increased connections in the frontal cortex in the CORT group were also seen with single-linkage distance matrices. Although the CORT group showed a similar trend in local and global connectivity (i.e., more localized and less global connectivity) in all frequency bands versus the VEH group, there were some differences in the connectivity pathways between the groups.

The dynamics of coupled oscillatory systems from each frequency band are useful for maintaining different functional sub-networks in a state of heightened competition, which can be stabilized and changed by even slight modulation of sensory or internal signals (Razavi et al., 2013; Smith, 2005). The underlying temporally correlated patterns of frequency-specific brain oscillations or activities are still not understood fully, and thus their purposes remain unclear at this time. As future investigations delve deeper into the origins and possible functions of frequency-related brain EEG activities, we will be able to comprehensively investigate brain function within frequency-specific brain networks.

Previous neuroimaging studies of depression in human suggested bilaterally loose connection at visual cortex and decreased connectivity among somatosensory, parietal, and frontal cortices, which are consistent with our results (Desseilles et al., 2011; Marchand et al., 2013). However, those studies could neither reveal subnetworks forming before the final network nor trace multi-scale functional networks. Application of persistent brain network homology to human neuroimaging data will help dig out persistent topological features in the evolution of networks, which can improve our knowledge about the pathogenesis of depression.

To date, various animal models (e.g., CORT treatment, chronic restraint stress, inescapable foot-shock stress, chronic social defeat stress, chronic unpredictable mild stress) have been established to facilitate understanding of the pathophysiology of depression (O'Neil and Moore, 2003). Although not without limitations, certain depression-associated phenotypes can be reproduced independently and evaluated in a mouse model. The CORT-induced depression mouse model used in this study is known to reproduce human behaviors, such as despair, anhedonia, or helplessness, which are regarded as face validity and which can be reversed by antidepressant treatment (Ardayfio and Kim, 2006; David et al., 2009; Gourley et al., 2008). However, depression is a heterogeneous disorder of which the diagnostic criteria are partially subjective. Thus, we cannot generalize our findings to specific clinical impacts in depression patients. To enable translation of the results, further research on the persistent brain network homology of clinical depression is essential.

Conclusion

In this study, we investigated cortical functional networks from multiple cortical EEG signals of the CORT-induced depression mouse model,

and demonstrated substantially altered functional connectivity in the CORT model. Use of the persistent brain network homology approach that considered all networks over every possible threshold enabled identification and quantification of increased local and decreased global connectivity of complex brain networks in the CORT model. Furthermore, loose coupling of somatosensory and other cortical regions and compromised functional connectivity between visual and other cortical regions were also revealed, which might contribute to deficient filtering or processing of information within brain regions in depression. Our study suggests the utility of the persistent brain network homology approach for tracing the evolution of EEG functional connectivity in neuropathological brain mapping, as well as the compromised functional connectivity in the CORT-induced depression model.

Acknowledgments

This work was supported by the Korea Health 21 R&D grants (HI12C0035 and HI12C1838) funded by Ministry of Health and Welfare. This work was also supported by the Basic Science Research Program grant (NRF-2014R1A2A2A01002608) funded by Ministry of Science, ICT and Future Planning.

Appendix A. Supplementary data

Supplementary data to this article can be found online at http://dx.doi.org/10.1016/j.neuroimage.2014.07.040.

References

Ardayfio, P., Kim, K.S., 2006. Anxiogenic-like effect of chronic corticosterone in the light–dark emergence task in mice. Behav. Neurosci. 120, 249–256.
Banks, S.M., Kerns, R.D., 1996. Explaining high rates of depression in chronic pain: a diathesis–stress framework. Psychol. Bull. 119, 95–110.
Bohland, J.W., Bokil, H., Allen, C.B., Mitra, P.P., 2009. The brain atlas concordance problem: quantitative comparison of anatomical parcellations. PLoS One 4, e7200.
Breakspear, M., Terry, J.R., 2002. Topographic organization of nonlinear interdependence in multichannel human EEG. Neuroimage 16, 822–835.
Buckner, R.L., Sepulcre, J., Talukdar, T., Krienen, F.M., Liu, H., Hedden, T., Andrews-Hanna, J.R., Sperling, R.A., Johnson, K.A., 2009. Cortical hubs revealed by intrinsic functional connectivity: mapping, assessment of stability, and relation to Alzheimer's disease. J. Neurosci. 29, 1860–1873.
Currie, S.R., Wang, J., 2004. Chronic back pain and major depression in the general Canadian population. Pain 107, 54–60.
David, O., Cosmelli, D., Friston, K.J., 2004. Evaluation of different measures of functional connectivity using a neural mass model. Neuroimage 21, 659–673.
David, D.J., Samuels, B.A., Rainer, Q., Wang, J.W., Marsteller, D., Mendez, I., Drew, M., Craig, D.A., Guiard, B.P., Guilloux, J.P., Artymyshyn, R.P., Gardier, A.M., Gerald, C., Antonijevic, I.A., Leonardo, E.D., Hen, R., 2009. Neurogenesis-dependent and -independent effects of fluoxetine in an animal model of anxiety/depression. Neuron 62, 479–493.
Davidson, R.J., 2004. What does the prefrontal cortex "do" in affect: perspectives on frontal EEG asymmetry research. Biol. Psychol. 67, 219–233.
Davidson, R.J., Lewis, D.A., Alloy, L.B., Amaral, D.G., Bush, G., Cohen, J.D., Drevets, W.C., Farah, M.J., Kagan, J., McClelland, J.L., Nolen-Hoeksema, S., Peterson, B.S., 2002a. Neural and behavioral substrates of mood and mood regulation. Biol. Psychiatry 52, 478–502.
Davidson, R.J., Pizzagalli, D., Nitschke, J.B., Putnam, K., 2002b. Depression: perspectives from affective neuroscience. Annu. Rev. Psychol. 53, 545–574.
Dawson, K.A., 2004. Temporal organization of the brain: neurocognitive mechanisms and clinical implications. Brain Cogn. 54, 75–94.
DeRubeis, R.J., Siegle, G.J., Hollon, S.D., 2008. Cognitive therapy versus medication for depression: treatment outcomes and neural mechanisms. Nat. Rev. Neurosci. 9, 788–796.
Desseilles, M., Schwartz, S., Dang-Vu, T.T., Sterpenich, V., Ansseau, M., Maquet, P., Phillips, C., 2011. Depression alters "top-down" visual attention: a dynamic causal modeling comparison between depressed and healthy subjects. Neuroimage 54, 1662–1668.
Drevets, W.C., Price, J.L., Furey, M.L., 2008. Brain structural and functional abnormalities in mood disorders: implications for neurocircuitry models of depression. Brain Struct. Funct. 213, 93–118.
Ferrarini, L., Veer, I.M., Baerends, E., van Tol, M.J., Renken, R.J., van der Wee, N.J.A., Veltman, D.J., Aleman, A., Zitman, F.G., Penninx, B.W.J.H., van Buchem, M.A., Reiber, J.H.C., Rombouts, S.A.R.B., Milles, J., 2009. Hierarchical functional modularity in the resting-state human brain. Hum. Brain Mapp. 30, 2220–2231.
Fingelkurts, A.A., Fingelkurts, A.A., Kahkonen, S., 2005. Functional connectivity in the brain — is it an elusive concept? Neurosci. Biobehav. Rev. 28, 827–836.
Fox, M.D., Snyder, A.Z., Vincent, J.L., Corbetta, M., Van Essen, D.C., Raichle, M.E., 2005. The human brain is intrinsically organized into dynamic, anticorrelated functional networks. Proc. Natl. Acad. Sci. U. S. A. 102, 9673–9678.
Friston, K.J., 2000. The labile brain. I. Neuronal transients and nonlinear coupling. Philos. Trans. R. Soc. Lond. B Biol. Sci. 355, 215–236.
Friston, K.J., Frith, C.D., Liddle, P.F., Frackowiak, R.S., 1993. Functional connectivity: the principal-component analysis of large (PET) data sets. J. Cereb. Blood Flow Metab. 13, 5–14.
Gourley, S.L., Wu, F.J., Taylor, J.R., 2008. Corticosterone regulates pERK1/2 map kinase in a chronic depression model. Ann. N. Y. Acad. Sci. 1148, 509–514.
Haig, A.R., Gordon, E., De Pascalis, V., Meares, R.A., Bahramali, H., Harris, A., 2000. Gamma activity in schizophrenia: evidence of impaired network binding? Clin. Neurophysiol. 111, 1461–1468.
He, B.J., Shulman, G.L., Snyder, A.Z., Corbetta, M., 2007a. The role of impaired neuronal communication in neurological disorders. Curr. Opin. Neurol. 20, 655–660.
He, B.J., Snyder, A.Z., Vincent, J.L., Epstein, A., Shulman, G.L., Corbetta, M.A., van Buchem, J.H., Reiber, S.A. Rombouts, Milles, J., 2007b. Breakdown of functional connectivity in frontoparietal networks underlies behavioral deficits in spatial neglect. Neuron 53, 905–918.
Jeon, D., Kim, S., Chetana, M., Jo, D., Ruley, H.E., Lin, S.Y., Rabah, D., Kinet, J.P., Shin, H.S., 2010. Observational fear learning involves affective pain system and $Ca_v1.2$ Ca^{2+} channels in ACC. Nat. Neurosci. 13, 482–488.
Jung, S., Seo, J.S., Kim, B.S., Lee, D., Jung, K.H., Chu, K., Lee, S.K., Jeon, D., 2013. Social deficits in the AY-9944 mouse model of atypical absence epilepsy. Behav. Brain Res. 236, 23–29.
Kessler, R.C., Berglund, P., Demler, O., Jin, R., Koretz, D., Merikangas, K.R., Rush, A.J., Walters, E.E., Wang, P.S., National Comorbidity Survey R., 2003. The epidemiology of major depressive disorder: results from the National Comorbidity Survey Replication (NCS-R). JAMA 289, 3095–3105.
Kessler, R.C., Berglund, P., Demler, O., Jin, R., Merikangas, K.R., Walters, E.E., 2005. Lifetime prevalence and age-of-onset distributions of DSM-IV disorders in the National Comorbidity Survey Replication. Arch. Gen. Psychiatry 62, 593–602.
Kito, S., Pascual-Marqui, R.D., Hasegawa, T., Koga, Y., 2014. High-frequency left prefrontal transcranial magnetic stimulation modulates resting EEG functional connectivity for gamma band between the left dorsolateral prefrontal cortex and precuneus in depression. Brain Stimul. 7, 145–146.
Lee, H., Kang, H., Chung, M.K., Kim, B.N., Lee, D.S., 2012. Persistent brain network homology from the perspective of dendrogram. IEEE Trans. Med. Imaging 31, 2267–2277.
Leistritz, L., Weiss, T., Bar, K.J., De VicoFallani, F., Babiloni, F., Witte, H., Lehmann, T., 2013. Network redundancy analysis of effective brain networks: a comparison of healthy controls and patients with major depression. PLoS One 8, e60956.
Leuchter, A.F., Cook, I.A., Hunter, A.M., Cai, C., Horvath, S., 2012. Resting-state quantitative electroencephalography reveals increased neurophysiologic connectivity in depression. PLoS One 7, e32508.
Marchand, W.R., Lee, J.N., Johnson, S., Gale, P., Thatcher, J., 2013. Differences in functional connectivity in major depression versus bipolar II depression. J. Affect. Disord. 150, 527–532.
Murray, F., Smith, D.W., Hutson, P.H., 2008. Chronic low dose corticosterone exposure decreased hippocampal cell proliferation, volume and induced anxiety and depression like behaviours in mice. Eur. J. Pharmacol. 583, 115–127.
Olbrich, S., Trankner, A., Chittka, T., Hegerl, U., Schonknecht, P., 2014. Functional connectivity in major depression: increased phase synchronization between frontal cortical EEG-source estimates. Psychiatry Res. 222, 91–99.
O'Neil, M.F., Moore, N.A., 2003. Animal models of depression: are there any? Hum. Psychopharmacol. 18, 239–254.
Patten, S.B., 2001. Long-term medical conditions and major depression in a Canadian population study at waves 1 and 2. J. Affect. Disord. 63, 35–41.
Paxinos, G., Franklin, K., 2012. Paxinos and Franklin's the Mouse Brain in Stereotaxic Coordinates. Academic Press. ISBN: 978-0-12-391057-8.
Price, J.L., Drevets, W.C., 2010. Neurocircuitry of mood disorders. Neuropsychopharmacology 35, 192–216.
Razavi, N., Jann, K., Koenig, T., Kottlow, M., Hauf, M., Strik, W., Dierks, T., 2013. Shifted coupling of EEG driving frequencies and FMRI resting state networks in schizophrenia spectrum disorders. PLoS One 8, e76604.
Ressler, K.J., Mayberg, H.S., 2007. Targeting abnormal neural circuits in mood and anxiety disorders: from the laboratory to the clinic. Nat. Neurosci. 10, 1116–1124.
Rubinov, M., Knock, S.A., Stam, C.J., Micheloyannis, S., Harris, A.W.F., Williams, L.M., Breakspear, M., 2009. Small-world properties of nonlinear brain activity in schizophrenia. Hum. Brain Mapp. 30, 403–416.
Seminowicz, D.A., Mayberg, H.S., McIntosh, A.R., Goldapple, K., Kennedy, S., Segal, Z., Rafi-Tari, S., 2004. Limbic-frontal circuitry in major depression: a path modeling metanalysis. Neuroimage 22, 409–418.
Shafi, M.M., Westover, M.B., Fox, M.D., Pascual-Leone, A., 2012. Exploration and modulation of brain network interactions with noninvasive brain stimulation in combination with neuroimaging. Eur. J. Neurosci. 35, 805–825.
Smith, S.J., 2005. EEG in neurological conditions other than epilepsy: when does it help, what does it add? J. Neurol. Neurosurg. Psychiatry 76 (Suppl. 2), ii8–ii12.

Stam, C.J., Breakspear, M., van Cappellen van Walsum, A.M., van Dijk, B.W., 2003. Nonlinear synchronization in EEG and whole-head MEG recordings of healthy subjects. Hum. Brain Mapp. 19, 63–78.
Suhhova, A., Bachmann, M., Aadamsoo, K., Võhma, Ü., Lass, J., Hinrikus, H., 2009. EEG coherence as measure of depressive disorder. 22, 353–355.
Sun, Y., Hu, S., Chambers, J., Zhu, Y., Tong, S., 2011. Graphic patterns of cortical functional connectivity of depressed patients on the basis of EEG measurements. Conf. Proc. IEEE Eng. Med. Biol. Soc. 2011, 1419–1422.
van der Staay, F.J., Arndt, S.S., Nordquist, R.E., 2009. Evaluation of animal models of neurobehavioral disorders. Behav. Brain Funct. 5, 11.
van Wijk, B.C.M., Stam, C.J., Daffertshofer, A., 2010. Comparing brain networks of different size and connectivity density using graph theory. PLoS One 28 (5(10)), e13701.